

Highlights

Investigation of Limited Detection Schemes for Light Scattering of Optically Trapped Asymmetric Particles

Dan Maciver, Praveen Parthasarathi, Leo Lue, Jan Sefcik, Mark Haw

- Asymmetric microsphere dimers can undergo complex dynamics including full inversions in the presence of a trapping potential, depending sensitively on the size ratio of the spheres making up the dimer.
- Orientations can be inferred from scattering signals through classification by a combination of neural networks and Bayesian inference.
- Signal error has a significant effect on the performance of the neural network, which can be countered via biasing of the prior distribution.
- Future applications include continuous processes where trapped particle characteristics such as size and shape are changing with time.

Investigation of Limited Detection Schemes for Light Scattering of Optically Trapped Asymmetric Particles

Dan Maciver^{a,*}, Praveen Parthasarathi^a, Leo Lue^a, Jan Sefcik^a, Mark Haw^a

^a*Department of Chemical Engineering, University of Strathclyde, 75 Montrose Street, Glasgow, G1 1XL, Scotland*

Abstract

While optical trapping is a well understood method for force transduction and detection, further characterisation of trapped entities using light-scattering poses a two-fold challenge — one experimental, concerning the optimal arrangement of light detectors to gather data, and the other theoretical, involving solving of the inverse light scattering problem in order to interpret this data. Experimentally, combining static light scattering techniques with optical trapping poses significant engineering challenges due to the space constraints in a conventional optical trapping setup. We propose here a plausible scenario of detecting scattered light from an optically trapped asymmetric microstructure using a novel, multi-angle, optical-fibre based detection scheme and demonstrate how a Bayesian inference based analysis of the data, combined with a neural-network trained on data simulated to mimic light scattering detection signals in such scenarios, may be used for solving the inverse light scattering problem and characterising complex trapped entities. To demonstrate the method we discuss its application to measuring the instantaneous orientations of a trapped asymmetric microsphere dimer. We argue that the method can be extended to determine any characteristics of the trapped microstructure that influence the light scattering pattern.

Keywords: Optical Trapping, Light Scattering, Measurements, Bayesian Statistics

1. Introduction

Since their invention in the late 1980s, optical tweezers have found application in experiments ranging from single molecule biophysics [1] to testing the fundamental assumptions of quantum mechanics [2], thanks mainly to the ability of the tweezer to transduce and detect forces on the order of a few pico-newtons. Going beyond forces, further structural, dynamic and chemical characterisation of complex trapped entities could provide useful information, as demonstrated in areas such as metrology [3] and colloidal aggregation [4]. Spectroscopic techniques such as Raman scattering [5] have been used for chemical characterisation of trapped objects, while dynamical characterisation has been demonstrated using data from tweezer's Quadrant Photo Detector (QPD) by following the centre-of-mass Brownian motion of the trapped entity [6] and measuring rotation of the centre-of-mass[7]. A recent work aimed at characterising trapped entities demonstrated how neural networks maybe trained to distinguish between optically trapped micro-beads of different size and material by means of a principal component analysis of the forward scattered light detected using a QPD [8]. A more direct, albeit cumbersome attempt at detecting scattered light from trapped biological cells was attempted in [9] where the experimental cuvette was placed inside an elliptical mirror that directed light scattered from the trapped biological-cell onto a photodetector via a rotating aperture that helped select the scattering-angle. Thus, past studies on optical trapping have focused rather heavily on particle-tracking but not particle-characterisation.

While both [8] [9] demonstrate some ability to characterise trapped entities, [8] is perhaps best suited to characterise micron-sized particles and [9] talks about an experimental setup that is difficult to adopt and

*Corresponding author

Email address: Daniel.Maciver.2016@uni.strath.ac.uk (Dan Maciver)

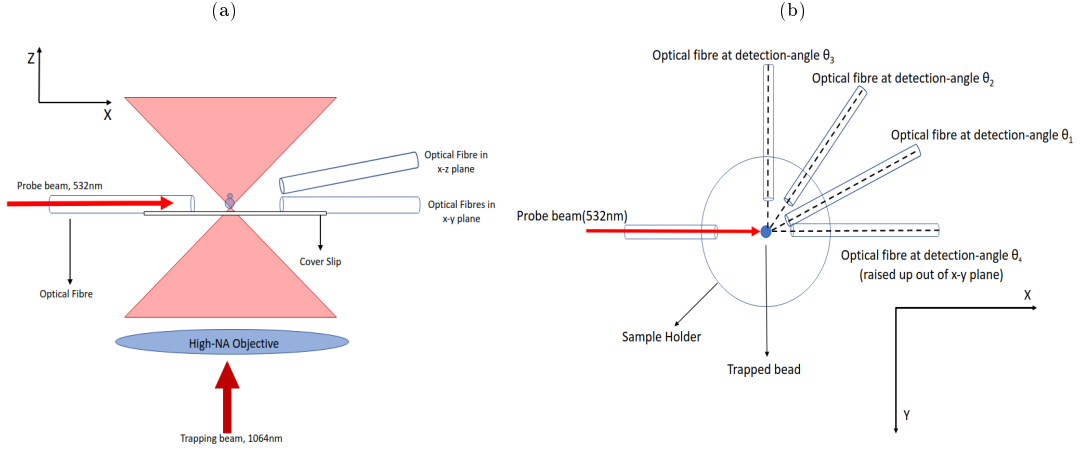


Figure 1: Proposed experimental set up for scattering measurements from an object in an optical trap. The probe beam for scattering measurements is incident perpendicular to the trapping laser propagation direction. a) Side view. b) Top view. Note that three of the detector fibres are co-planar with the incident probe beam, while the fourth detector is placed out of the plane (see text).

suffers from a low-bandwidth that might not be best suited for monitoring dynamics. A light scattering detection scheme built around an optical trap that is both easy to implement and has the advantage of high-bandwidth was demonstrated by Safran and co-workers in [10], where a single-mode optical fibre was aligned to detect the scattered light from a trapped bead and study its Brownian motion. While this provided dynamical information, structural information about the trapped bead was precluded as the measurement was obtained only at a single angle. Furthermore, the main drawback to a single fibre detection scheme is that it struggles to characterise isotropically scattering particles. This limits its application to biological matter as the internal structure of many cells makes them inherently isotropic scatterers [9]. In this work, we propose a scheme that expands on the technique in [10] to detect scattered light simultaneously at a number of angles (Figure 1), combined with a novel Bayesian inference-based analysis technique to enable interpretation of the resulting multi-angle data as well as optimisation to provide maximal information from the signal.

To demonstrate the analysis, we study a simple, illustrative example of an isotropic scattering entity *i.e.* an asymmetric dimer. As a paradigmatic example of extracting structural/dynamic information from the resulting scattering data, we explore how to estimate the dimer’s instantaneous orientation from the scattering signals using Bayesian inference, as well as how to optimise the analysis by implementing ‘prior knowledge’ to obtain the most reliable estimate. As an example of the relatively sparse literature on measuring orientations of complex trapped objects, ref. employs imaging to study the orientation of trapped dimers: scattering can give more quantitative and potentially more rapid time-resolved information, but only of course if the scattering signals can be interpreted. Here, we first train a neural network to effectively identify the mapping between scattering signals and dimer orientation, by calculating the scattering signal from a simulated asymmetric dimer undergoing Brownian motion in an optical trap and mapping to the known instantaneous orientation of the simulated dimer. We then show how Bayesian inference can be used to optimise extraction of the true dimer orientation from the light scattering signals. Furthermore we demonstrate how the model can be fine tuned in situations where measurement uncertainty becomes significant.

2. Methodology

2.1. Brownian Simulation

We use the Brownian OT package developed by Fung *et al* [11] to simulate the motion of an asymmetric dimer (Figure 2a) within an optical trap. Brownian OT combines MSTM [12] and “Optical Tweezer Toolbox”

(*ott*) [13] to simulate the motion of arbitrary shaped sphere clusters. We simulate the motion of a dimer trapped in a highly focused Gaussian beam by calculating the optical forces imparted by the laser, and the Brownian forces imparted by the surrounding fluid. MSTM provides the necessary T-matrix to compute the optical force via *ott*. The Brownian force is found by computing the dimer's diffusion tensor according to the analytical solutions provided by Nir and Acrivos [14]. For a dimer of arbitrary sized spheres the diffusion tensor - which describes the Cartesian forces and torques - is a 6×6 matrix:

$$\begin{pmatrix} F_x \\ F_y \\ F_z \\ T_x \\ T_y \\ T_z \end{pmatrix} = \begin{pmatrix} a_1 & 0 & 0 & 0 & d_1 & 0 \\ 0 & a_1 & 0 & -d_1 & 0 & 0 \\ 0 & 0 & a_1 + a_2 & 0 & 0 & 0 \\ 0 & -d_1 & 0 & b_1 & 0 & 0 \\ d_1 & 0 & 0 & 0 & b_1 & 0 \\ 0 & 0 & 0 & 0 & 0 & b_1 + b_2 \end{pmatrix} \begin{pmatrix} v_{k0} - V_k \\ v_{k0} - V_k \\ v_{k0} - V_k \\ \omega_x - \Omega_x \\ \omega_y - \Omega_y \\ \omega_z - \Omega_z \end{pmatrix} \quad (1)$$

where each matrix component is scaled by a factor of $k_B T / \pi \eta$. When both sphere's are identically sized - as in Fung *et. al*'s work - d_1 goes to zero; however for our work with asymmetric spheres these components are significant enough to be considered. We simulated a silica dimer ($n = 1.45$) in a suspension of water ($n_{med} = 1.33$) over the course of 10 s with a simulation time step of 1×10^{-5} s.

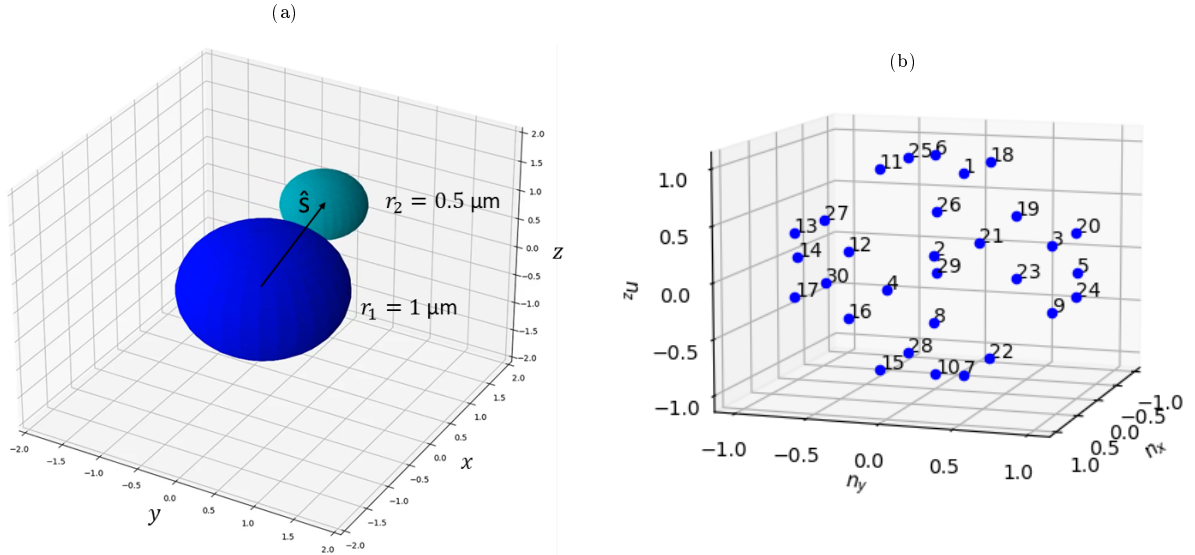


Figure 2: (a) Example dimer in orientation \hat{s} , (b) 30 Reference orientations represented by vectors pointing from $[0,0,0]$ to each point

2.2. Orientation estimation from scattering measurements

For our simulated dimer in the optical trap (Fig. 2a), we can define at any point in time a unit vector \hat{s} pointing from the centre of the larger sphere to the centre of the smaller sphere. A plane wave 'probe' laser, perpendicular to the trapping laser, is incident on the dimer, generating a scattering pattern dependent on the dimer's orientation $I(\hat{s}, \theta)$ which is computed using MSTM. To represent the experimental set up consisting of a set of optical fibres recording scattered light, we choose four angles ($\theta_1, \theta_2, \theta_3, \theta_4$) and record the calculated intensity at each angle θ_k , $I(\hat{s}, \theta_k)$.

Our goal is to determine the orientation of the trapped dimer based on the scattering data $I(\hat{n}, \theta_k)$. Rather than aim immediately for an exact estimate of the dimer's orientation, for the purposes of interpretation of the scattering and optimisation of the measurement setup it is more convenient to discretize the possible orientation space into a number of possible reference orientations, which we can then use as 'classification

categories' in a neural network methodology to map scattering data to orientation (see below for further discussion). Here we choose $n_{ref} = 30$ reference orientations $\hat{\mathbf{n}}_\alpha$ evenly distributed on a unit sphere [15] (Figure 2b) leading to a maximum nearest-neighbour spacing between two neighbouring reference orientations of 0.895 radians. Using MSTM we compute the raw intensities at each of the measurement angles that would be generated by a dimer in each reference orientation, $I(\hat{\mathbf{n}}_\alpha, \theta_k)$. While the number and position of detection fibres is technically arbitrary there are several constraining factors that limit our ability to infer useful information from the trapped object, see Section 3.1 for a detailed breakdown of our choice of detection angles. The raw intensities are normalized according to:

$$y_k(\hat{\mathbf{n}}_\alpha) = \frac{I(\hat{\mathbf{n}}_\alpha, \theta_k) - \langle I(\hat{\mathbf{n}}, \theta_k) \rangle}{\langle I^2(\hat{\mathbf{n}}, \theta_k) \rangle - \langle I(\hat{\mathbf{n}}, \theta_k) \rangle^2} \quad (2)$$

where the denominator is simply the standard deviation across the set of values $I(\hat{\mathbf{n}}, \theta_k)$. The reference orientations, raw intensities, and scaled signals are given in Tables A1 and A2.

Note that the collected scattering signals are not necessarily simply related to their associated reference orientations: as is well known from such examples of the inverse scattering problem, the mapping between the structural space of variables such as orientation, and the space of scattering signals may be highly complex. Even if the orientation space is divided evenly between reference orientation the subsequent signal space ends up being appearing mixed making simple comparisons of signals useless for inferring information on the particle. Nevertheless, at least where the uncertainty in signal measurements is low (see below), we can predict the orientation from the scattering by utilising computational techniques such as neural networks. We thus utilised the Python machine learning program *scikit-learn* to build a neural network for identifying the dimer's orientation from its light scattering signal. The network was trained by generating a database of random orientation vectors, calculating the corresponding light scattering signals, and then using the network to estimate the probability of a given signal coming from a dimer in a given reference orientation. The network's loss function was evaluated and used to improve the estimation, the network being trained until the improvement in the loss function was less than 0.0001. Importantly, the estimation provided by the neural network can be improved further by accounting for any prior information we know about the dimer, utilising Bayesian inference to update the neural network's estimation:

$$p(\hat{\mathbf{n}}_\alpha | y_k(\hat{\mathbf{s}})) = \frac{p(y_k(\hat{\mathbf{s}}) | \hat{\mathbf{n}}_\alpha) p(\hat{\mathbf{n}}_\alpha)}{p(y_k(\hat{\mathbf{s}}))} \quad (3)$$

where $p(\hat{\mathbf{n}}_\alpha)$ and $p(y_1, y_2, y_3)$ are the prior estimates of the distributions of particle orientations and instantaneous signals, respectively. *Without* any prior evidence we must assume that the orientation prior of the dimer $p(\hat{\mathbf{n}}_\alpha)$ is uniform. However, inference about the dimer's possible current orientation from knowledge of previous measurements can be used to inform our estimate of $p(\hat{\mathbf{n}}_\alpha)$ (see Section 3.2). The latter prior $p(y)$ is the probability of measuring a signal (y_1, y_2, y_3) . This is given by taking the discrete integral over the collection of reference orientations:

$$p(y_1, y_2, y_3, y_4) = \sum_{\alpha=1}^{n_{ref}} p(y_1, y_2, y_3, y_4 | \hat{\mathbf{n}}_\alpha) p(\hat{\mathbf{n}}_\alpha) \quad (4)$$

From (3) we obtain the key result, a mass probability distribution denoting the probability that our dimer is in orientation $\hat{\mathbf{n}}_\alpha$ given a measured signal (y_1, y_2, y_3) , *i.e.* an estimated mapping from scattering measurement to orientation estimate.

2.3. Calculation of error

To evaluate the above estimation of dimer orientation from scattering signal, we use a Brownian simulation of a dimer in the optical trap (Section 2.1) to compare estimated most probable reference orientation, derived from the dimer's scattering through Eq. (3), with the dimer's known *actual* orientation $\hat{\mathbf{s}}$. MSTM provides calculated light scattering from the simulated dimer $I(\hat{\mathbf{s}}, \theta)$ and we use (2) to obtain normalized values

at each measurement angle θ_k , $y_1(\hat{\mathbf{s}})$, $y_2(\hat{\mathbf{s}})$, $y_3(\hat{\mathbf{s}})$, from which we obtain $p(\hat{\mathbf{n}}_\alpha \parallel y_1, y_2, y_3)$. Because we know the actual orientation $\hat{\mathbf{s}}$ we can measure the error in the model's estimate by comparing the reference orientation closest to $\hat{\mathbf{s}}$, denoted as $\hat{\mathbf{n}}_{best}$, with the most probable predicted orientation from Eq. (3). An ideal result would be one where the probability distribution is 0 for every $\hat{\mathbf{n}}$ apart from $\hat{\mathbf{n}}_{best}$:

$$p_{best} = \begin{cases} 1 & \text{when } \hat{\mathbf{n}}_\alpha = \hat{\mathbf{n}}_{best} \\ 0 & \text{anywhere else} \end{cases} \quad (5)$$

In reality the distribution from Eq. (3) will assign some non-zero probability to every reference orientation, leading to some level 'confidence' in orientation prediction, which can be quantified by calculating the Kullback-Leibler divergence K_l between the two distributions:

$$K_{l,\#}(p_{best} \parallel p(\hat{\mathbf{n}}_\alpha | y_1, y_2, y_3)) = p_{best} \ln \left[\frac{p_{best}}{p(\hat{\mathbf{n}}_{best} | y_1, y_2, y_3)} \right] \quad (6)$$

where a larger value of K_l indicates that our model is less confident in its prediction of the dimer's orientation. The divergence K_l thus illustrates the 'spread' in the estimated dimer orientation probability — a distribution strongly peaked at some value would give us more confidence in that value than a near-uniform distribution where the scattering measurement could imply a wide range of possible orientations — but it does not directly indicate our estimate's actual accuracy.

3. Results and Discussion

3.1. Minimal number of detectors

The exact number of detectors was initially assumed to be arbitrary, in that it made no difference to our estimate whether we used 2 angles or 200. For practical purposes it seemed beneficial that we demonstrate our method works for a minimal number of detection angles, as geometric constraints come into play when trying to install a high number of detection fibres around a single point.

Initially we tried capturing scattered light only in the x-y plane as to simulate the detectors all being placed on a glass cover slip. The results of this estimate are shown below. As can be seen from Figure the neural network performs particularly poorly in this situation, seemingly jumping back and forth between different reference orientation at random. We found that when all three detectors are in the same plane the expected signal can appear identical despite the dimer being in completely different orientations. This is shown in Figure which plots the expected signals from 30 reference orientations, each point is labelled with its corresponding reference orientation, the fact that points have multiple labels shows that the dimer's scattering is indistinguishable in these two reference orientation. More specifically, if the detectors are placed say in the x-y plane then only when the dimer is pointed nearly fully upright will the expected signal be entirely unique. This is illustrative of the difficulty behind the inverse light scattering problem; as attributing the measured signal will not reveal any new information about the entity unless we can remove uncertainty around other aspects of the scatterer.

To remedy this we raise the third detector out of the x-y plane; as such the expected signals from each reference orientation is unique. With only three detectors the difference in expected signals can appear insignificant; by adding a 4th detector we can differentiate signals more reliably, improving the neural networks performance. In line with our goal of making this method viable in a laboratory setting we decided not to increase the number of detectors further than 4.

3.2. Testing the Model

Using our simulation from Section 2.1 we simulated the motion of a silica dimer ($n = 1.59$) trapped in water ($n = 1.33$) within a 5 mW optical trap. The trapping laser is 1064nm NIR focused through a 1.25 NA objective. The dimer is comprised of two tangent spheres with radii $1\mu m$ and $0.5\mu m$ respectively. We simulated the first 10 seconds of motion, calculating the orientation and position every 1 ms.

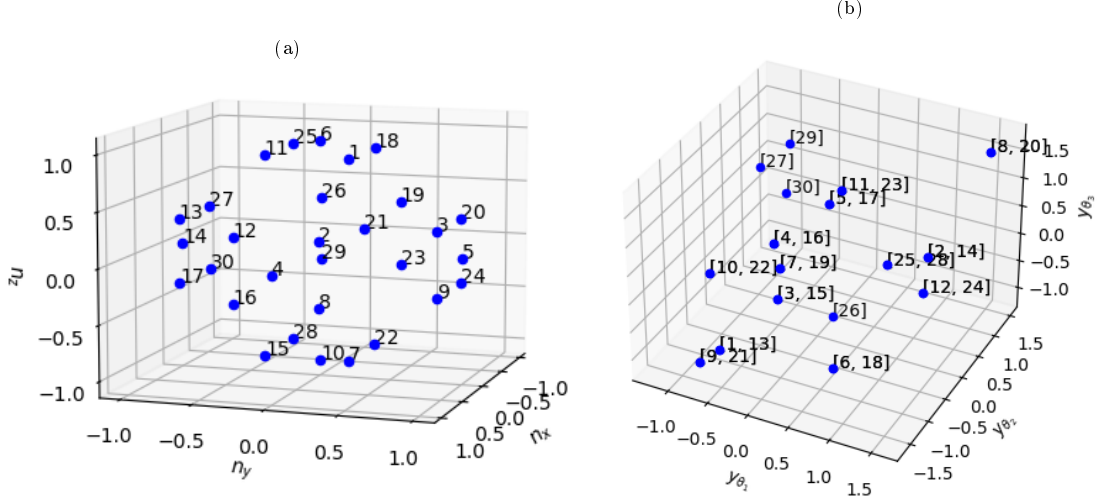


Figure 3: (a) 30 Reference orientations represented by vectors pointing from [0,0,0] to each point (b) Expected signal for each reference orientation, some signals map to multiple reference orientation and are labelled as such.

We applied Eq. (3), taking the reference orientation with the highest probability as our estimate of the dimer's instantaneous orientation $\hat{\mathbf{n}}_{est}$. To visualise the model's performance we plotted the radial distance between our estimation $\hat{\mathbf{n}}_{est}$ and the dimer's *actual* instantaneous orientation $\hat{\mathbf{s}}$ versus time. For comparison, we also plotted the radian distance between the dimer's instantaneous orientation and the closest reference orientation, denoted $\hat{\mathbf{n}}_{best}$. The dotted line indicates the maximum radian distance (0.896 radians) between two *neighbouring* reference orientations: if we are under this line then we know our estimate is at least neighbouring the best result. Assuming a uniform prior of the reference orientations $p(\hat{\mathbf{n}}_\alpha)$ the neural network's predictions ($\hat{\mathbf{n}}_{est}$ from Eq. (3)) are at times reasonable, but there are significant large and random jumps away from the correct result (Fig. 4).

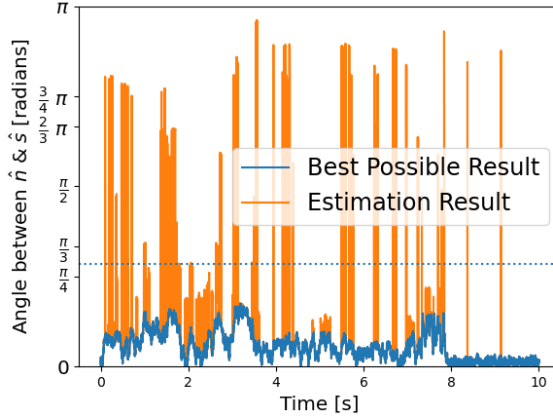


Figure 4: Model's estimation of dimer orientation over the simulation time, assuming uniform prior $p(\hat{\mathbf{n}}_\alpha)$. Blue line denotes the best result we can achieve (the reference orientation $\hat{\mathbf{n}}_{best}$ that is closest to the actual orientation), orange line denotes the result provided by eq 3: where the orange line is not visible, the model's prediction agrees with $\hat{\mathbf{n}}_{best}$. Horizontal dotted line denotes maximum spacing between two neighbouring $\hat{\mathbf{n}}_\alpha$.

One reason we observe such large jumps in orientation estimated from scattering signals is that there is

no simple correlation between the 'distance in scattering space' between scattering signals from two different orientations, and their separation in orientation space: even a large change in orientation can involve a small change in scattering. Combining this fact with use of a uniform prior, indicating essentially no knowledge of how orientation should behave, there is no constraint on how much estimated orientation can change from time-step to time-step. To improve the estimation we can therefore use knowledge of the physical limitations of the object in the trap and its dynamics, imposing a more physically grounded prior, accounting in this case for the fact that the motion of the dimer is limited due to the trap stiffness. Here the prior of the reference orientations $p(\hat{\mathbf{n}}_\alpha)$ was redefined at each time step as a Boltzmann distribution of the physical distance between the previous estimate $\hat{\mathbf{n}}_{est}(t - \Delta t)$ and each reference orientation $\hat{\mathbf{n}}_\alpha$. Put simply, we are reweighing our estimation based on the size of rotation required, with smaller movements being favoured over large movements:

$$p(\hat{\mathbf{n}}_\alpha) = \frac{e^{\beta(\hat{\mathbf{n}}_\alpha \cdot \hat{\mathbf{n}}_{est}(t - \Delta t))}}{\sum_{\alpha=1}^{n_{ref}} e^{\beta(\hat{\mathbf{n}}_\alpha \cdot \hat{\mathbf{n}}_{est}(t - \Delta t))}} \quad (7)$$

Here β is a weighting factor describing the dimer's freedom of motion within the trap. As shown in Figure 5 implementation of Eq (7) helps significantly reduce the large random excursions of estimated orientation away from the 'best' result.

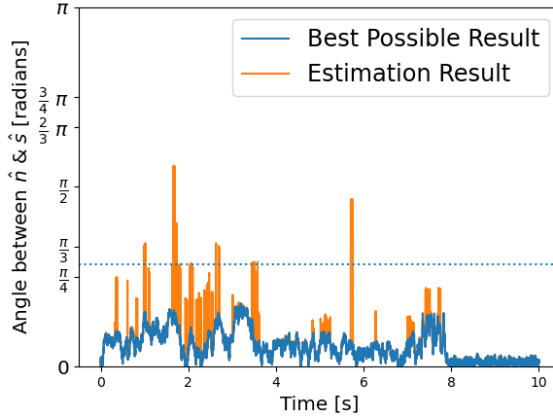


Figure 5: Estimation of dimer orientation with $p(\hat{\mathbf{n}}_\alpha)$ defined by Eq (7). Blue line denotes the best result we can achieve, orange line denotes the result provided by eq 3. Dotted line denotes spacing between two neighbouring reference orientations $\hat{\mathbf{n}}_\alpha$ (see Section 2.2).

The simulation data from Section 2.1 was used to evaluate our model's performance — covered in Section 2.3. By summing the divergence of each measurement across the entire simulation we get an evaluation of how well the model performed in estimating the dimer's orientation. To compare the effects of changing certain parameters on the performance of our model we compare our result of $K_{l,total}$ to a worst case scenario and evaluate how much it improves upon this, denoted as $F(K_l)$:

$$K_{l, total} = \sum_{\# = 1}^{timesteps} K_{l, \#} \quad (8)$$

$$K_{l, worst} = \sum_{\# = 1}^{timesteps} \ln \left[\frac{1}{1/n_{ref}} \right] \quad (9)$$

$$F(K_l) = \frac{K_{l, worst}}{K_{l, total}} \quad (10)$$

The worst case scenario is akin to randomly choosing a reference orientation at each time step. The greater the value of $F(K_I)$, the better our model's confidence is in characterising the dimer's motion. Because our model is dependent on several parameters we need to a sophisticated method for understanding how these parameters correlate with $F(K_I)$.

3.3. Impact of measurement noise on model predictions

So far a key assumption of the neural network implementation is that the detected scattering signal has no uncertainty associated with it. In reality of course scattering signals will always have some non-zero measurement noise. This can be attributed to a variety of factors, from a measurement bias in the detector, to the Brownian motion of the dimer itself. To explore the impact of measurement uncertainty on orientation estimation model performance we introduce a Gaussian noise to the measured signal:

$$I(\hat{\mathbf{s}}) = I(\hat{\mathbf{s}}) \pm \epsilon I(\hat{\mathbf{s}}) \quad (11)$$

where ϵ is the percentage error associated with the scattering signal. Figure 6 shows the performance of the model at a range of ϵ using in-plane detector angles 15° , 55° , 90° and out-of-plane detector at 75° , with β set to 1:

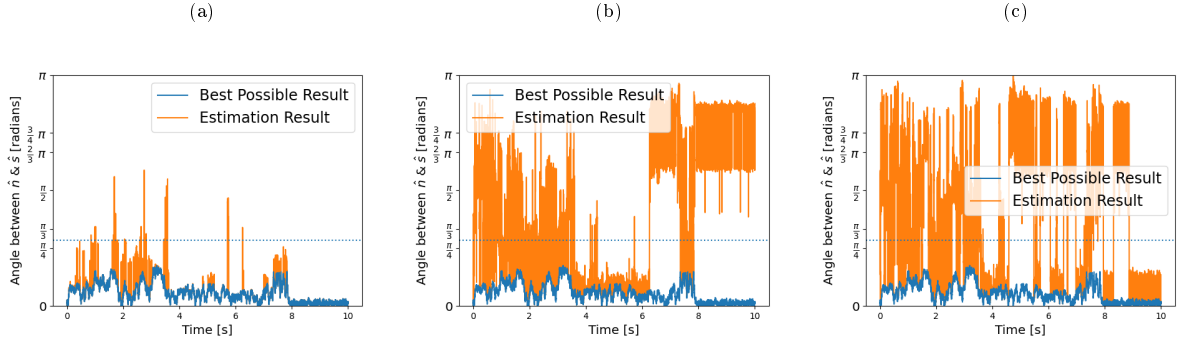


Figure 6: Model prediction for signal error of (a) 1% [$F(K_I) = 1.174$], (b) 15% [$F(K_I) = 0.606$], and (c) 25% [$F(K_I) = 0.457$].

As can be seen from Figure 6, the inclusion of signal noise quickly leads to a decrease in the model's performance. This is due to an inherent feature of the inverse scattering problem: two distinct regions in orientation space can become heavily intertwined and thus no longer well separated when mapped to intensity space (even though the mapping remains continuous): so even small uncertainties in the scattering data can lead to large 'mistakes' in the choice of orientation by the neural network. (Indeed if this was not the case the inverse scattering problem would be quite simple.)

To reduce the effects of the signal noise we took the time average of the expected signal over several time steps and then had our neural network estimate the orientation based on the average signal. This allowed us to mitigate the effects of any signal error that may persist in light scattering measurements, as shown below.

Diagnostics of optically trapped biological cells often have to contend with large fluctuations in scattering signals due to the fact that their light scattering ability is isotropic. Understanding the dynamics of these cells within an optical trap are essential for better characterisation methods. Our method demonstrates that we can extract orientational dynamics from a trapped entity via modelling its scattering in MSTM and then applying it to a raw scattering signal.

4. Conclusion

We have developed a method for measuring the dynamics of an optically-trapped 'complex object' based purely on limited measurements of the object's light scattering at a small number of detection angles. We demonstrate the method using the orientation of an asymmetric dimer as the dynamical variable and

object of interest, but in principle the model can be applied to any characteristic that impacts the light scattering pattern produced by a trapped entity. The MSTM package is a flexible tool for calculating the light scattering of complex objects using a representation of the object as a set of micro-particles, enabling training of a neural network to enable categorisation of the mapping between scattering and trapped object characteristics. By taking account of knowledge about the physically realistic behaviour of the trapped object and the characteristics of the trap (which impact the dynamics of the object), the Bayesian inference method can be refined to provide a reliable estimation of object characteristics of interest, even in the presence of measurement noise. Fundamentally the inverse scattering problem is difficult to solve since the mapping between object characteristics and scattering can be highly complex: but Bayesian inference based on neural network estimation of the mapping provides a powerful method for practical applications, extending the use of optical trapping beyond measuring microscopic force response toward detailed structural and dynamic information about complex trapped entities.

Here we simplify the problem somewhat by employing a relatively small finite number of 'reference orientations' to map between scattering and dimer orientation: the precision of estimation could be improved by utilising a greater number of reference orientations, although there remains a balance between the realisable precision of orientation estimate and the noise level of the scattering measurement. Another avenue to further explore would be using the method to optimise the choice of detection angles, essentially to find the region in the mapping between measured scattering and orientation that offers the best degree of confidence through optimal separation of scattering signals for distinct orientations. For *sequences* of data such as dynamic measurements, a further potential enhancement would be to consider more complex correlations based on prior expectations of the dynamics. Here already we improve the method using a non-uniform prior based on only the immediately previous measurement in time (see Section 2.2): considering more detailed correlations such as multiple previous timesteps is likely to further enhance the reliability of the estimation.

Acknowledgement. The authors thank the support for this research from the funding provided by the Leverhulme Trust.

Disclosures. The authors declare no conflict of interest.

References

- [1] C. J. Bustamante, Y. R. Chemla, S. Liu, and M. D. Wang, "Optical tweezers in single-molecule biophysics," *Nature Reviews Methods Primers*, vol. 1, Mar 2021.
- [2] Z.-q. Yin, T. Li, X. Zhang, and L. Duan, "Large quantum superpositions of a levitated nanodiamond through spin-optomechanical coupling," *Physical Review A*, vol. 88, no. 3, p. 033614, 2013.
- [3] Y. Arita, S. H. Simpson, P. Zemánek, and K. Dholakia, "Coherent oscillations of a levitated birefringent microsphere in vacuum driven by nonconservative rotation-translation coupling," *Science advances*, vol. 6, no. 23, p. eaaz9858, 2020.
- [4] M. M. Burns, J.-M. Fournier, and J. A. Golovchenko, "Optical matter: crystallization and binding in intense optical fields," *Science*, vol. 249, no. 4970, pp. 749–754, 1990.
- [5] P. Gupta and S. Ahlawat, "Raman spectroscopic studies on optically trapped red blood cells," in *International Conference on Fibre Optics and Photonics*, pp. S3D-2, Optica Publishing Group, 2014.
- [6] L. Friedrich and A. Rohrbach, "Tuning the detection sensitivity: a model for axial backfocal plane interferometric tracking," *Optics letters*, vol. 37, no. 11, pp. 2109–2111, 2012.
- [7] Y. Yifat, J. Parker, T.-S. Deng, S. K. Gray, S. A. Rice, and N. F. Scherer, "Facile measurement of the rotation of a single optically trapped nanoparticle using the diagonal ratio of a quadrant photodiode," *ACS Photonics*, vol. 8, no. 11, pp. 3162–3172, 2021.
- [8] I. A. Carvalho, N. A. Silva, C. C. Rosa, L. C. Coelho, and P. A. Jorge, "Particle classification through the analysis of the forward scattered signal in optical tweezers," *Sensors*, vol. 21, no. 18, p. 6181, 2021.
- [9] D. Watson, N. Hagen, J. Diver, P. Marchand, and M. Chachisvilis, "Elastic light scattering from single cells: orientational dynamics in optical trap," *Biophysical journal*, vol. 87, no. 2, pp. 1298–1306, 2004.
- [10] R. Bar-Ziv, A. Meller, T. Tlusty, E. Moses, J. Stavans, and S. A. Safran, "Localized dynamic light scattering: Probing single particle dynamics at the nanoscale," *Physical Review Letters*, vol. 78, p. 154–157, Jan 1997.
- [11] W. Vigilante, O. Lopez, and J. Fung, "Brownian dynamics simulations of sphere clusters in optical tweezers," *Optics Express*, vol. 28, p. 36131, Nov 2020.

- [12] D. W. Michael I. Mishchenko, Larry D. Travis, “T-matrix computations of light scattering by nonspherical particles: A review,” *Light scattering by Non-Spherical Particles*, vol. 55, pp. 535–575, 1996.
- [13] I. C. D. Lenton, T. A. Nieminen, V. L. Y. Loke, A. B. Stilgoe, Y. Hu, G. Knöner, A. M. Brańczyk, N. R. Heckenberg, and H. Rubinsztein-Dunlop, “Optical tweezers toolbox.” <https://github.com/ilent2/ott>, 2020.
- [14] A. Nir and A. Acrivos, “On the creeping motion of two arbitrary-sized touching spheres in a linear shear field,” *Journal of Fluid Mechanics*, vol. 59, p. 209–223, Jun 1973.
- [15] G. C. Reythor, *Numerical methods for radiative heattransfer*. Doctoral thesis, Universitat Politècnica de Catalunya, 2006.

Appendix

Table A1: Reference Orientations vector components*

α	$\hat{\mathbf{n}}_{\alpha, x}$	$\hat{\mathbf{n}}_{\alpha, y}$	$\hat{\mathbf{n}}_{\alpha, z}$
1	0.29588	0.29588	0.90825
2	0.90825	0.29588	0.29588
3	0.29588	0.90825	0.29588
4	1.00000	0.00000	0.00000
5	0.00000	1.00000	0.00000
6	0.00000	0.00000	1.00000
7	0.29588	0.29588	-0.90825
8	0.90825	0.29588	-0.29588
9	0.29588	0.90825	-0.29588
10	0.00000	0.00000	-1.00000
11	0.29588	-0.29588	0.90825
12	0.90825	-0.29588	0.29588
13	0.29588	-0.90825	0.29588
14	0.00000	-1.00000	0.00000
15	0.29588	-0.29588	-0.90825
16	0.90825	-0.29588	-0.29588
17	0.29588	-0.90825	-0.29588
18	-0.29588	0.29588	0.90825
19	-0.90825	0.29588	0.29588
20	-0.29588	0.90825	0.29588
21	-1.00000	0.00000	0.00000
22	-0.29588	0.29588	-0.90825
23	-0.90825	0.29588	-0.29588
24	-0.29588	0.90825	-0.29588
25	-0.29588	-0.29588	0.90825
26	-0.90825	-0.29588	0.29588
27	-0.29588	-0.90825	0.29588
28	-0.29588	-0.29588	-0.90825
28	-0.90825	-0.29588	-0.29588
30	-0.29588	-0.90825	-0.29588

*Orientation vector points from centre of sphere 1 to centre of sphere 2.

Table A2: Raw intensities I_k^* and scaled intensities y_k

α	$I(\hat{\mathbf{n}}_\alpha, 15^\circ)$	$I(\hat{\mathbf{n}}_\alpha, 55^\circ)$	$I(\hat{\mathbf{n}}_\alpha, 90^\circ)$	$y(\hat{\mathbf{n}}_\alpha, 15^\circ)$	$y(\hat{\mathbf{n}}_\alpha, 55^\circ)$	$y(\hat{\mathbf{n}}_\alpha, 90^\circ)$
1	5.6777	0.0180	0.0122	-0.3137	-0.6242	-0.4838
2	5.2364	0.0088	0.0102	-0.5663	-0.8951	-0.7826
3	9.0297	0.0141	0.0234	1.6044	-0.7378	1.1622
4	4.5187	0.0459	0.0221	-0.9770	0.2062	0.9695
5	8.5891	0.0392	0.0244	1.3523	0.0060	1.3031
6	7.1799	0.0377	0.0142	0.5458	-0.0383	-0.1886
7	5.0015	0.0071	0.0095	-0.7007	-0.9468	-0.8792
8	4.8573	0.0578	0.0095	-0.7832	0.5604	-0.8794
9	9.0184	0.0618	0.0273	1.5979	0.6774	1.7262
10	4.6351	0.1536	0.0221	-0.9103	3.4040	0.9641
11	5.6777	0.0180	0.0122	-0.3137	-0.6242	-0.4838
12	5.2364	0.0088	0.0102	-0.5663	-0.8951	-0.7826
13	9.0297	0.0141	0.0234	1.6044	-0.7378	1.1622
14	8.5891	0.0392	0.0244	1.3523	0.0060	1.3031
15	5.0015	0.0071	0.0095	-0.7007	-0.9468	-0.8792
16	4.8573	0.0578	0.0095	-0.7832	0.5604	-0.8794
17	9.0184	0.0618	0.0273	1.5979	0.6774	1.7262
18	7.1549	0.0408	0.0076	0.5315	0.0532	-1.1580
19	4.0546	0.0085	0.0076	-1.2425	-0.9035	-1.1576
20	5.9164	0.0122	0.0188	-0.1771	-0.7945	0.4765
21	4.2902	0.0103	0.0142	-1.1077	-0.8510	-0.1890
22	7.9307	0.1005	0.0102	0.9754	1.8281	-0.7835
23	4.0693	0.0414	0.0122	-1.2342	0.0718	-0.4840
24	6.5422	0.0506	0.0234	0.1809	0.3446	1.1622
25	7.1549	0.0408	0.0076	0.5315	0.0532	-1.1580
26	4.0546	0.0085	0.0076	-1.2425	-0.9035	-1.1576
27	5.9164	0.0122	0.0188	-0.1771	-0.7945	0.4765
28	7.9307	0.1005	0.0102	0.9754	0.1005	0.0102
29	4.0693	0.0414	0.0122	-1.2342	0.0718	-0.4840
30	6.5422	0.0506	0.0234	0.1809	0.3446	1.1622

* I_k values are calculated using MSTM package.